AD-A278 394

N PAGE

Form Approved
OMB No. 0704-0188

Public repo
gathering a
collection o
Davis Highv

our per response, including the time for reviewing instructions, searching existing data sources,
tion of information. Send comments regarding this burden estimate or any other aspect of this
ton Headquarters Services, Directorate for Information Operations and Reports, 1215 Jefferson
ent and Budget, Paperwork Reduction Project (0704-0188), Washington DC 20503

1. AGEN

3. REPORT TYPE AND DATES COVERED
FINAL REPORT 01 Feb 91 - 30 Nov 93

4. TITLE AND SUBTITLE
Advanced Materials Processing for Integrated-Optic Frequency Doubling Systems

5. FUNDING NUMBERS
2301 CS

(2)

6. AUTHOR(S)
R A Rubino, D. E. Cullen

7. PERFORMING ORGANIZATION NAME(S) AND ADDRESS(ES)
United Technology Rsch Center
East Harford, CT 06108

8. PERFORMING ORGANIZATION REPORT NUMBER
AFOSR-TR- 94 0237

9. SPONSORING / MONITORING AGENCY NAME(S) AND ADDRESS(ES)
AFOSR/NE
110 Duncan Avenue, Suite B115
BOLLING AFB WASHINGTON DC 20332-0001

10. SPONSORING / MONITORING AGENCY REPORT NUMBER
F49620-91-C-0022

DTIC
ELECTE
APR 20 1994
S F D

11. SUPPLEMENTARY NOTES

12a. DISTRIBUTION / AVAILABILITY STATEMENT
APPROVED FOR PUBLIC RELEASE: DISTRIBUTION IS UNLIMITED

12b. DISTRIBUTION CODE

13. ABSTRACT (Maximum 200 words)
The purpose of this two year program has been to investigate novel materials processing techniques for the purpose of producing highly efficient, nonlinear waveguide frequency doublers compatible with the integration of compact semi-conductor sources. As yet, practical, direct conversion, semiconductor sources of blue-light, have still to be proven, thereby motivating the research of waveguide second-harmonic generation, (SHG).

DTIC

14. SUBJECT TERMS

15. NUMBER OF PAGES

16. PRICE CODE

| 17. SECURITY CLASSIFICATION OF REPORT | 18. SECURITY CLASSIFICATION OF THIS PAGE | 19. SECURITY CLASSIFICATION OF ABSTRACT | 20. LIMITATION OF ABSTRACT |
|---|---|---|---|
| UNCLASSIFIED | UNCLASSIFIED | UNCLASSIFIED | UL (UNLIMITED) |

NSN 7540-01-280-5500

Standard Form 298 (Rev 2-89)
Prescribed by ANSI Std 239-18
298-102

UNITED TECHNOLOGIES RESEARCH CENTER
East Hartford, Connecticut 06108

**Final Report**
**R94-970053-1**

# *Advanced Material Processing for Integrated-Optic Frequency Doubling Systems*

**AFOSR Program F49620-91-C-0022**

**R. A. Rubino**

**D. E. Cullen**

R94-970053-1

Final Report

# *Advanced Material Processing for Integrated-Optic Frequency Doubling Systems*

## TABLE OF CONTENTS

## 1.0 EXECUTIVE SUMMARY

The purpose of this two year program has been to investigate novel materials processing techniques for the purpose of producing highly efficient, non-linear waveguide frequency doublers compatible with the integration of compact semi-conductor sources. As yet, practical, direct conversion, semi-conductor sources of blue-light, have still to be proven, thereby motivating the research of waveguide second-harmonic generation, (SHG).

Well known for its large non-linear coefficient and its widespread use as a superior opto-electronic integrated circuit (OEIC) material, lithium niobate, $LiNbO_3$, and lithium tantalate, $LiTaO_3$, shows great promise for this task. This material does not poses adequate birefringence to allow for conventional phase matching however, and requires the fabrication of a phase compensating periodic structure along the waveguide. Theoretically, the SHG conversion efficiency of this quasi-phase matching (QPM) technique can be quite high (70% of conventional phase matching), given: **(1) the phase grating is first order, (2) the domain-reversal profile is rectangular and is sufficiently deep to ensure good overlap with the guided waves and (3) the postional tolerance of the domain walls is well below (<1%) the domain period (3.6μm).**

We report two novel processing techniques developed for the unique poling requirements of x-cut niobate and tantalate: (1) Phase-I — laser induced thermal poling and (2) Phase-II — e-beam poling. Throughout this work, X-cut material was used since this orientation allows for the integration of superior OEIC modulaters and is readily expandable to applications involving arrays of sources.

Although the laser poling technique circumvents the period/depth limitations of diffusion-based poling techniques developed for z-cut material, the wall angle of the laser poled domains, by virtue of this also being a diffusion (of heat) process, significantly reduces the conversion efficiency attainable with this approach. Moreover, the domains are "written" serially, which we have found can lead to poor grating periodicity and is not amenable to high volume production of these devices. **SHG experiments using QPM gratings fabricated using the laser poling method were characterized by: (1) broad acceptance bandwidths (~10nm), (2) low conversion efficiencies (3.6% $W \cdot cm^{-2}$) and (3) excessive scattering loss in the region of the thermally poled material.**

Recognizing its inherent limitations, the laser thermal poling technique was abandoned in Phase II in favor of an e-beam writing technique that has shown great promise in the processing of z-cut material. The e-beam technique developed at UTRC for processing of x-cut material begins with ion milling a 3μm high ridge mesa in the direction of the QPM waveguide. For all intents and purposes, electrons injected into the -z face of this mesa ridge, "see" the electrode on the +z face completely analogous to the highly successful z-cut e-beam process. Although, timing and founding did not allow waveguides to be processed in the e-beam polled material, we present experimental results which indicate this technique capable of mass producing QPM gratings with the qualities essential for high conversion efficiency SHG.

## 2.0 INTRODUCTION

The development of a short-wavelength visible coherent light sources is an important milestone for numerous technologies such as optical data storage, xerography, space and underwater communications. At present, a semiconductor laser capable of producing visible radiation at green or blue wavelengths has not been demonstrated. While materials such as zinc selenide (ZnSe) and silicon carbide (SiC) have been identified as promising materials in which to fabricate blue-emitting semiconductor laser diodes, the ability to define high quality p-n junctions in these materials has proven extremely difficult [23,24]. Therefore, non-linear frequency doubling of infrared radiation from AlGaAs semiconductor diode lasers is an attractive and viable alternative for producing coherent blue light.

Because of their ability to maintain high optical intensities over long interaction lengths, optical waveguides offer an efficient geometrical structure in which to perform second harmonic generation. In particular, lithium niobate ($LiNbO_3$), with its large nonlinear susceptibility and well developed waveguide technology, has proven to be an attractive waveguide medium in which to perform nonlinear frequency conversion. However, $LiNbO_3$ and $LiTaO_3$ does not have adequate birefringence to achieve conventional phase matching for second harmonic generation (SHG) of green and blue light. As a result, a quasi-phase-matching (QPM) technique has been employed in $LiNbO_3$ waveguides to generate blue light.[4] In the QPM technique, the phase velocity mismatch between the waveguide modes at the fundamental and second harmonic frequencies is compensated by periodically reversing the sign of the nonlinear susceptibility. The QPM technique allows phase matching of any interaction within the transparency range of the $LiNbO_3$ and $LiTaO_3$ crystal using the largest nonlinear coefficient of the material.

Quasi-phase-matched frequency doubling has been demonstrated in periodically poled $LiTaO_3$ waveguides, resulting in the generation of up to 12 mW of blue light for a continuous-wave infrared input power of 190 mW.[25] While this initial demonstration of blue-light generation via frequency doubling in periodically poled, $LiNbO_3$ waveguides is very encouraging, practical applications require higher system efficiencies, in a format compatible with volume production processes.

In this final report we document our efforts at UTRC focusing on material processing of optically non-linear waveguides for frequency doubling systems. Specifically, this two year effort has been directed towards QPM SHG in x-cut niobate and tantalate material involving:

- the development of a novel laser-assisted thermoelectric poling technique for improved QPM grating fabrication and domain-inversion profile in the first half of the program
- and later in the program, the development of an e-beam poling domain inversion technique compatible with large scale production methods.

## 3.0 TECHNICAL DISCUSSION

The trend toward optical media for data storage and the need for higher bit densities has spurred interest in the development of short-wavelength light sources. Of the potential candidate technologies, frequency doubling of GaAlAs/GaAs lasers seems to offer the most viable alternative. While demonstrations thus far have been promising, they fall short of offering the efficiency and output intensities necessary for practical implementation. The overall efficiency and subsequent output intensity of a SHG system is strongly dependent on (I) the strength of the effective nonlinear coefficient, (2) the power handling capability of the waveguide medium, and (3) the amount of fundamental power coupled into the waveguide structure as will be discussed in the section that follows.

### 3.1 Quasi-Phase-Matched Second-Harmonic Generation in $LiNbO_3$ and $LiTaO_3$ Waveguides

Frequency doubling of infrared radiation from a semiconductor diode laser to generate blue light has been demonstrated in $LiNbO_3$ planar and channel waveguides. Despite its large nonlinear susceptibility, lithium niobate and tantalate does not have adequate birefringence to achieve conventional phase-matching for second harmonic generation of blue light. However, quasi-phase-matching, QPM, in integrated-optic waveguides has emerged as a viable alternative. First described by Somekh and Yariv in 1972 [25], quasi-phase-matching utilizes a periodic reversal of the sign of the nonlinear coefficient to prevent an accumulated phase mismatch between the interacting fundamental and second harmonic waves.

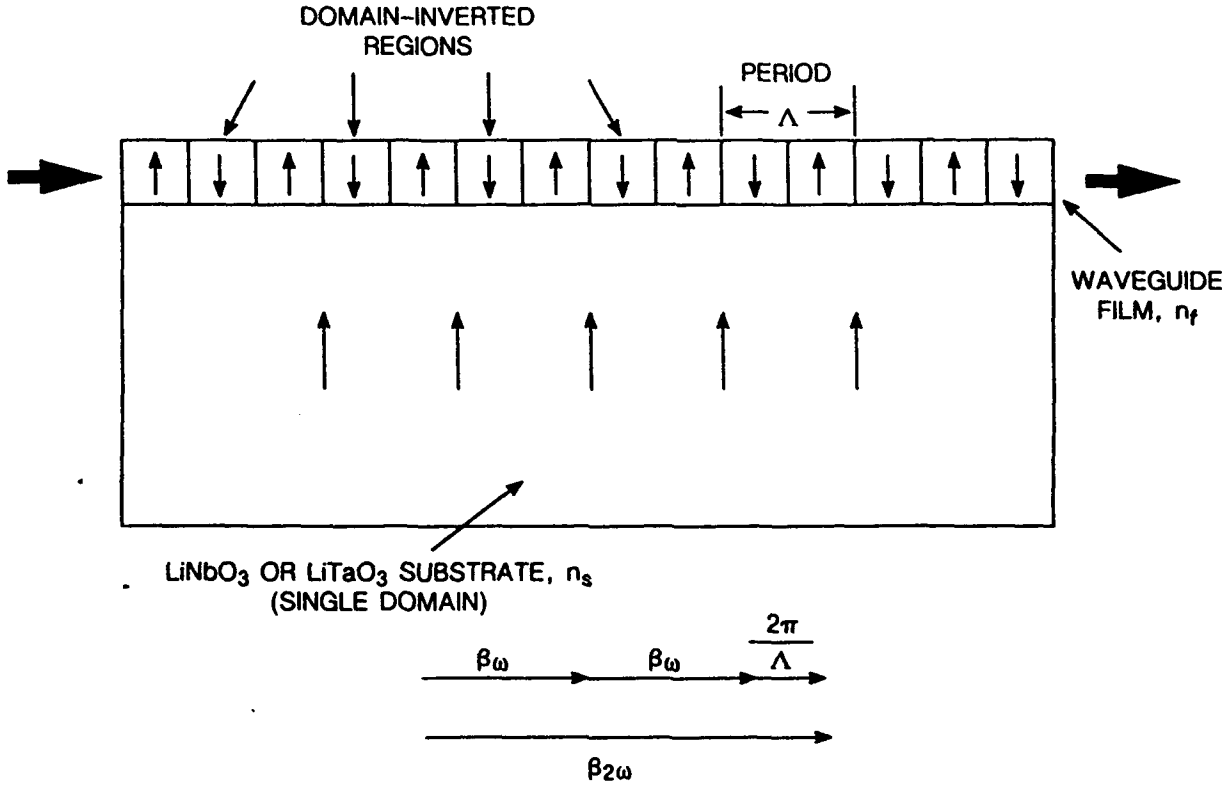


**Fig. 3-1. Quasi-phase-matched waveguide in $LiNbO_3$ or $LiTaO_3$ for efficient frequency doubling.**

Figure 3-1 is an idealized cross-sectional illustration of a periodically poled QPM waveguide fabricated on z-cut $LiNbO_3$ The basic period L of the domain-inverted grating, which corresponds to the coherence length, is determined from the following QPM condition:

$$\beta_{2\omega} = 2\beta_{\omega} + \frac{2\pi}{\Lambda} \qquad (3\text{-}1)$$

where , $\beta_{\omega}$ and $\beta_{2\omega}$ are the propagation constants of the guided modes at the fundamental and second-harmonic frequencies, respectively. Higher-order gratings in which the grating period is equal to an integer multiple, n, of the basic grating period can also be used for second-harmonic generation. However, the maximum conversion efficiency for these higher-order gratings is reduced by a factor of $1/n^2$ when compared to the conversion efficiency of the basic period.[26] In the case of lithium niobate or lithium tantalate, QPM enables the use of the largest nonlinear coefficient, $d_{33}$, for an interaction between z-polarized electric fields.

In the nondepleted pump approximation, the frequency-conversion efficiency from $\omega$ to $2\omega$ for a QPM integrated-optic waveguide is:

$$\frac{P(2\omega)}{P(\omega)} = \frac{2\omega^2}{[n(\omega)]^2 \cdot n(2\omega)} \left(\frac{\mu_o}{\varepsilon_o}\right)^{3/2} \cdot d^2_{eff} l^2 \frac{P(\omega)}{Wt} \qquad (3\text{-}2)$$

where ω is the fundamental angular frequency, P(2ω ) is the guided-mode output power at frequency 2ω, P(ω)) is the guided-mode input power at frequency ω , l is the length of the frequency-doubling grating, $d_{eff}$ is the effective nonlinear coefficient, c is the speed of light, n(ω) and n(2ω) are the refractive indices of the waveguide film at ω and 2ω, and W and t are the lateral and transverse dimensions of the waveguide region.

Several important observations can be made from an examination of Eq. (3-2). First, the frequency conversion efficiency is proportional to the power density of the guided mode at the fundamental frequency, P(ω)/Wt. Hence, the second-harmonic power that is generated is proportional to the square of the fundamental power coupled into the waveguide. Efficient coupling of infrared power into a nonlinear waveguide device is therefore essential for an efficient frequency-doubled source of blue light. According to Eq. (3-2), the frequency conversion efficiency of a quasi-phase-matched device is also proportional to the square of the effective nonlinear coefficient, $d_{eff}$. This effective nonlinear coefficient differs from the nonlinear coefficient of the bulk material, $d_{NL}$, by a factor that is strongly dependent on the profile of the domain-inverted grating [25,27]. For the case of the ideal rectangular grating illustrated in Fig. 3-1, the two quantities are related by:

$$d_{eff} = \frac{2d_{NL}}{\pi} \qquad (3\text{-}3)$$

For a grating profile that differs from the ideal rectangular structure, the effective nonlinear coefficient can be significantly reduced from the value given in Eq. (3-3). Therefore, a quasi-phase-matched frequency-doubling system requires an optimized domain-inversion profile in order to efficiently generate blue-light.

To date, periodic domain inversion to produce quasi-phase-matched channel waveguides in $LiNbO_3$ has been demonstrated using several different substrate poling techniques. Specifically, periodically poled surface layers have been achieved through (1) in diffusion of a periodic grating of Ti into the C-face of a $LiNbO_3$ sample [4,6], (2) periodic out-diffusion of $Li_2$ through a patterned silicon dioxide mask [26,27], (3) electron beam writing through a suitable attenuation mask [11], and (4) a high temperature anneal technique that relies on creating reduced Curie temperature features via assisted proton exchange [28]. After production of the periodically poled surface layer in $LiNbO_3$, all of the fabrication techniques utilize the annealed proton-exchanged process to define channel waveguides in the $LiNbO_3$ substrate.

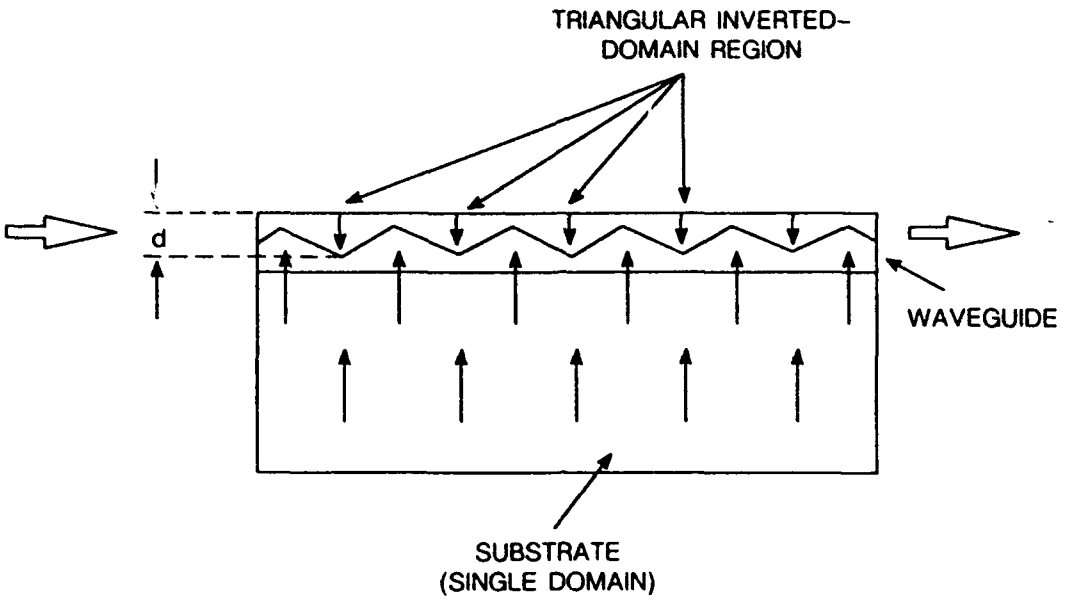


**Fig. 3-2. Triangular domain-inversion profile obtained by processes using Ti indiffusion or $LiO_2$ out-diffusion. The frequency-conversion efficiency of this structure is strongly dependent on the depth of the domain inversion, d, and is inherently lower than the efficiency of the rectangular profile in Fig. 3-1.**

For QPM efficient second-harmonic generation of blue light in $LiNbO_3$ waveguides, a first-order grating period of ~3 mm is required. The use of higher order gratings simplifies the grating fabrication process; however, this simplifed fabrication process comes at the expense of a reduced frequency conversion efficiency. Third order frequency-doubling gratings in $LiNbO_3$ have been demonstrated by using the Ti-indiffusion process, but these gratings yield low conversion efficiencies [4,5,6]. In addition, the presence of Ti within the $LiNbO_3$ waveguide significantly increases the likelihood of photo-refractive damage to the waveguide at the power levels necessary for efficient second-harmonic generation.

In the ideal QPM case illustrated in Fig. 3-1, the domain-inverted waveguide regions are rectangular in shape, in order to achieve a strong overlap between the domain-inverted regions and the guided mode. However, the currently employed processes for producing frequency-doubling gratings in $LiNbO_3$ and $LiTaO_3$ have resulted in triangular domain cross sections, illustrated in Fig. 3-2. For a triangular profile the angle between the domain boundary and the substrate surface is ~30°, which corresponds to crystallographic planes within the material. For the triangular domain profile, the conversion efficiency of the structure is extremely sensitive to the depth of the domain inversion, d. The position of the domain boundary with respect to the crystal surface must therefore be carefully controlled. However, a triangular boundary whose position has been carefully optimized still has a frequency-conversion efficiency four times smaller than that of an ideal rectangular structure [12].

Clearly, to ensure maximum SHG conversion effeciency, the phase grating must posses domains which are: (1) as rectangular as possible, (2) deep in comparison to the waveguide depth to guarantee good modal overlap and as will be discussed in section 4.1, (3) the grating periodicity must be carefully controlled. It is with these requirements in mind that the thermal-electric and e-beam poling techniques have been developed at UTRC.

## 4.1 Laser Thermo-Electric Processing of $LiNbO_3$ and $LiTaO_3$

Since beginning this work two years ago, QPM SHG has received much attention, most notably from Japanese researchers [1,2,3], as a viable method to produce compact blue sources for a variety of commercial applications. As a result of the increased developmental effort, a variety of novel poling schemes have been recently demonstrated. One of the best of these devices to date, fabricated by a diffusion defined domain/heat treatment technique, has produced 15mW of second harmonic output power. In spite of these results however, the continuing developmental work in order to find a process that not only yields a QPM grating with optimum profiles but one which is also compatible with large scale manufacturability, is testament to the relevancy of our work in this field. With the exception of e-beam poling techniques, **all of the other poling processes are diffusion based schemes and like the e-beam technique, are applicable to z-cut material only.** Hence, the motivation for developing a domain inversion technique for x-cut $LiNbO_3$ and $LiTaO_3$ which is not fundamentally limited by the period/depth profile typically achieved with diffusion based schemes, is as important today as it was a year ago.

To circumvent this inherent limitation, we proposed the use of a thermo-electric poling technique in which a small region of the wafer would be heated above its Curie temperature and the application of an external bias field would reorient the domain in the desired direction. From our perspective, this was perhaps the most intuitive poling mechanism as compared to the Ti diffusion, self poling technique as reported by Fejer et al. [4,5,6]. As illustrated in Fig. 4-1, our technique uses a wafer of x-cut $LiNbO_3$ or $LiTaO_3$, patterned with two electrodes separated by 200 μm. These electrodes traverse the entire length of the desired QPM grating in the y-direction. Processing is performed by irradiating the region to be poled by appropriately adjusting the intensity and spot size of an infrared beam having a wavelength which is absorbed by the material, such as 10.6 μm light from a $CO_2$ laser. In this way, the material surface temperature in the illuminated region can be raised above the Curie temperature, (1140°C and 610°C for niobate and tantalate respectively). Once heated, an electric bias of 200 volts is applied to one of the electrodes while the other is grounded, thereby producing an electric field which is either parallel or anti-parallel to the z-axis. The applied electric field orients the spontaneous ferroelectric polarization within the heated region exceeding the Curie temperature ($T_c$). After cooling below the $T_c$, the realignment is permanent.

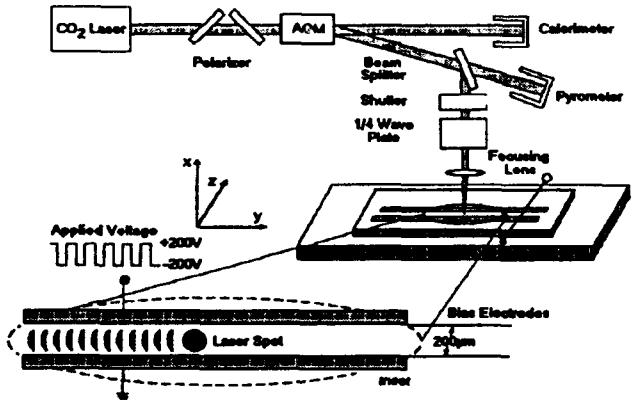


**Fig. 4-1. Schematic of thermal-electric poling setup showing how a QPM grating is fabricated using a focused $CO_2$ laser spot to heat a region of the substrate above $T_c$. Application of an electric field of 10,000V/cm poles the heated region in the desired direction.**

This process has several clear advantages over the various diffusion based schemes:

- The reversed domain retains all of the desired optical properties of the unpoled substrate. It has long been recognized that channel waveguides fabricated by Ti indiffusion yielded devices susceptible to optical damage at relatively low optical powers. By not relying on modification of the substrate chemistry, *the thermo-electric poling technique coupled with APE™ waveguides ensures optical damage thresholds on a par with the unpoled maternal.*
- *The thermo-electric process is reversible.* If, as a result of the poling process, a domain error is detected, the QPM grating can be re-processed to eradicate the mistake. This has distinct advantages when considering fabrication of arrays of doublers in which the array yield is the product of the individual doubler yields.

- *QPM gratings possessing domain wall profiles independent of the period length can be fabricated* with the thermo-electric poling technique.

Early on, it was realized that use of a laser poling technique in which the domain dimensions are determined by the laser spot size or by the use of a reflective masking technique, is in itself a diffusion technique and would impose severe limitations on the depth and profile of the individual domain dimensions. However, through utilization of the reversibility feature of this process, domains with extremely sharp transitions and dimensions appreciably smaller than the laser heating beam size, can be fabricated without the typical trade-off between period and domain depth normally encountered with diffusion techniques.

However, before these features could be realized, concerns regarding the applicability of the thermal technique to these materials, namely: (1) material survivability of thermal stresses associated with surface temperatures in excess of the Curie point (610°C and 1140°C for tantalate and niobate, respectively), (2) avoidance of self-poling as a consequence of the thermal gradient produced pyroelectric field and (3) optimization of poling parameters to give the most reproducible and best profile domain profile possible had to be formulated.

### 4.1.1 Thermal Model

From our previous work in laser annealing of APE™ waveguides, we have found that for small laser spot sizes, $LiNbO_3$ could be heated to high temperatures without permanent damage to the surface. In fact it was through this work, that 100μm diameter spots of molten $LiNbO_3$ were produced without obvious surface damage, which was the basis for the proposed thermal poling work. Although the melting point is not accompanied by material damage per se, the cooled molten region can be characterized by what looks like a "weld bead" as shown in Fig. 4-2, and is too rough to allow for subsequent waveguide processing. Hence, *the material's melting temperature represents an upper limit* for the thermal-electric poling technique. However, for $LiNbO_3$ this is problematical, since the proximity of the melting point for $LiNbO_3$ to its

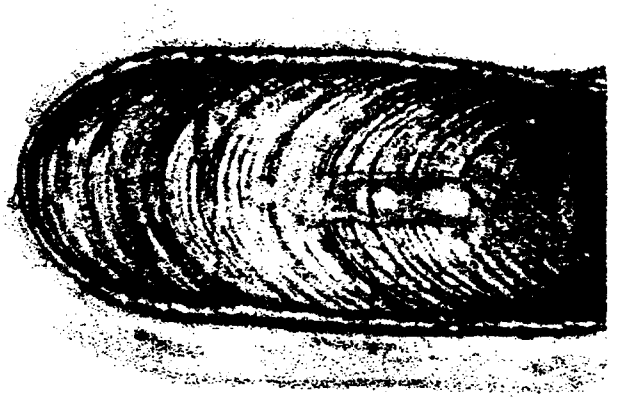

**Fig. 4-2. Molten region of $LiNbO_3$ formed by a scanned $CO_2$ beam. Note that other than the surface roughness of the "weld bead", there is no evidence of cracking in the sorrounding material.**

Curie temperature, (1253°C and 1140°C respectively) requires the implementation of an accurate thermal model to predict and control the optical power density to achieve the desired surface temperatures.

Fortunately, laser annealing and laser welding is a fairly mature field [7,8] and has recently seen applications in semiconductor processing [9,10]. For our purposes, applications involving semiconductors are of special interest, in that these materials closely approximate the thermal characteristics expected for both $LiNbO_3$ and $LiTaO_3$. For the steady state case, the semiconductor thermal model can be extended to the materials of interest and solved analytically by assuming some minor approximations. Specifically, both tantalate and niobate are characterized by fairly low reflection coefficients (~4%) at these wavelengths. This number is relatively temperature invariant [11], and for the purposes of our calculations we have assigned it as a constant. Furthermore, although the experimental data is sparse, one correctly concludes from the asymmetry of the phonon resonance spectra, that the thermal diffusivity and conductivity is direction dependent. However, the magnitude of the variation is small and since as a first approximation, we are primarily interested in the peak surface temperature rather than the gradient, we chose the thermal conductivity to be isotropic. Making these assumptions, the heat equation written as

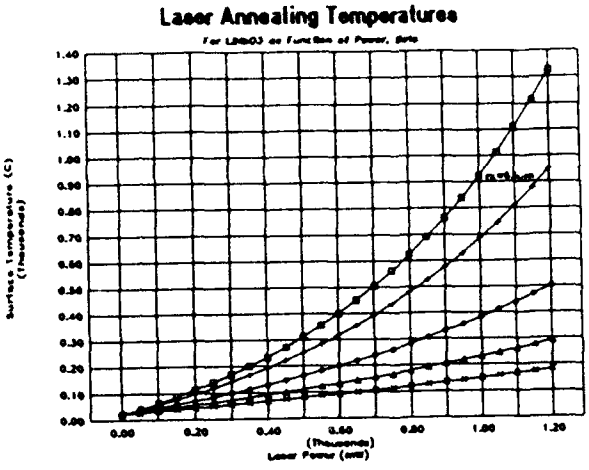


**Fig. 4-3. Peak surface temperature of $LiNbO_3$ as a function of $CO_2$ power and spot eccentricity normalized to a gaussion spot with $r_x$=63μm and β = 1, 2, 4, 8, 16.**

$$\frac{K(T)}{D(T)}\frac{\partial T}{t} - \nabla\cdot[K(T)\nabla T] = Q(x,y,z,t) \quad (4\text{-}1)$$

can be solved, by performing a Kirchoff transform to eliminate the temperature dependent thermal conductivity K(T). The solution of (4-1) is further simplified by assuming that the best (steepest) domain wall profiles will be obtained for the stationary beam case in which the thermal steady state is achieved. Hence, the thermal diffusivity, D(T), can be neglected and the problem can be solved analytically.

Solving the simplified heat equation by a Green's function method and introducing coordinates which are normalized to the characteristic radius of the irradiating Gaussian beam, the problem becomes a purely geometrical quantity which is generic to all materials and spot sizes. From the meager thermal conductivity data on these materials [9] and fitting the experimental data to a 1/T dependence, peak surface temperatures as a function of beam ellipticity and optical power density can be calculated. From Fig. 4-3 one notes that for spot sizes produced with $f^*$ 5 optics, relatively small $CO_2$ laser powers are required to achieve the Curie temperature, ($T_c$)

Since, QPM conversion efficiency is not only critically dependent on the domain depth profile but also the domain profile in the horizontal direction, calculations for poling schemes involving elliptical $CO_2$ spot profiles to increase the effective radius of curvature of the domain were also investigated. Ellipticities of β =1, 2, 4, 7.8, & 16 were used, where $\beta = r_y/r_x$. Since, the horizontal dimension of the QPM waveguides are no more than 5μm, use of a sufficiently large spot could achieve the same effect. Using the optics on hand, a 63μm spot was used for all QPM grating fabrication.

To verify our thermal model, a comparison between the point at which surface melting occurred and the predicted power level for this temperature for $LiNbO_3$, was found to correspond to within 5%. For niobate, the degree of accuracy required for our model is extremely important when considering the proximity of the melting point ($T_{mp}$) to $T_c$. From Fig. 4-3., the optical power required to achieve $T_c$ is 1.12 watts and $T_{mp}$ is 1.17 watts. From a practical perspective, 50 mW accuracy is readily achievable in the lab, however from a processing point of view, the domain depth profile (if one is to avoid the melting point) is extremely shallow.

This is a consequence of working with gaussian poling beam profiles. Constrained to using a poling power which produces a peak surface temperature just below $T_{mp}$, the resulting domain radius corresponding to the off-beam center distance where the optical power density barely achieves $T_c$, is quite small. Furthermore, from the first derivative of the intensity profile with respect to y, one notes that the temperature restrictions forces grating fabrication parameters which will yield domain wall positions susceptible to variations in beam power.

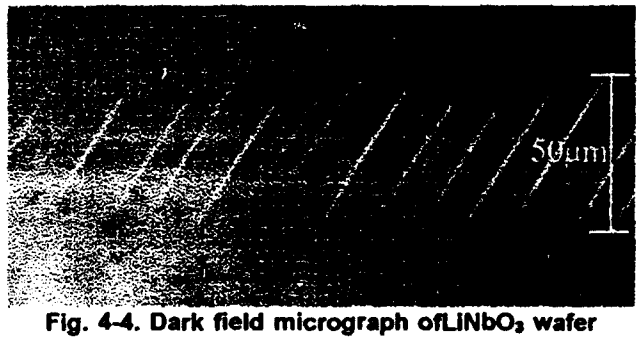


**Fig. 4-4. Dark field micrograph of$LiNbO_3$ wafer reveals sstress cracks after thermal poling process.**

### 4.1.2 Thermal-Electric Poling in $LiNbO_3$

These problems notwithstanding, the availability of high quality optical grade material and a factor of two improvement in the optical non-linearity over $LiTaO_3$, motivated an attempt at thermal poling of $LiNbO_3$. Using a step and repeat poling process whereby the $LiNbO_3$ wafer was exposed to a 1.16 watt (just below $T_{mp}$), 63μm beam for 2 seconds to achieve thermal steady state and then cooled for 2 seconds. The sample was then moved a distance corresponding to half the QPM grating period and re-exposed but with the poling bias field reversed. This procedure was repeated down the 3mm length of the grating. Using a dark field microscope to detect the residual strain associated with the inverted domains however, revealed that the laser irradiated region showed evidence of excessive strain and surface cracks as shown in Fig. 4-4. As a method to minimize the thermal gradient induced strain during laser poling, a small oven fitted with a ZnSe window to allow passage of the $CO_2$ beam and appropriate electrical feed-throughs was fabricated. However, in spite of elevating the wafer temperature to 300°C, the stress cracking could not be prevented. Furthermore, the pointing accuracy of the poling beam was appreciably perturbed due to imaging through the thermal turbulence set up by the hot oven. At this point thermal electric poling of $LiNbO_3$ was abandoned.

### 4.1.3 Thermal Poling of $LiTaO_3$

As with the niobate thermal model, the thermal conductivity of $LiTaO_3$ was assumed isotropic and the steady state problem was solved to yield Fig. 4-5. The temperature process range afforded by tantalate's $T_c$ of 610°C and its melting point at 1600°C not only relaxes the poling power control tolerance but also allows greater flexibility in choice of poling optical power density. From the temperature curves, one finds $T_c$ is achieved with 260 mW and $T_{mp}$ at 450 mW for a 63μm spot. *The large separation of $T_c$ and $T_{mp}$ for tantalate allows the QPM grating designer to pick a power density which: (1) minimizes the effect of power instability on domain wall position and (2) maximize the domain depth and achieve the best possible domain profile.*

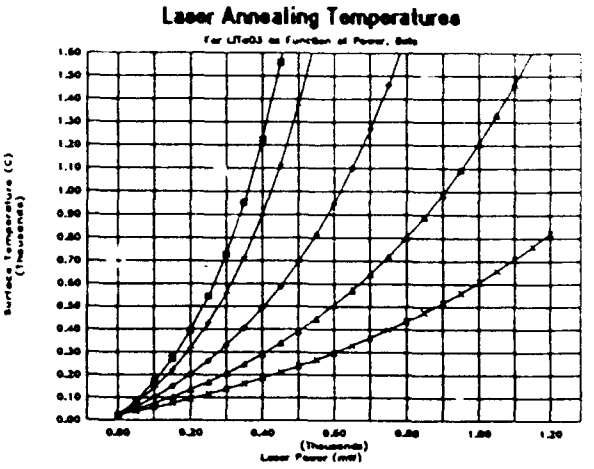


**Fig. 4-5. Peak surface temperature of $LiTaO_3$ as a function of $CO_2$ power and spot eccentricity normalized to a gaussian spot with $r_x$=63μm and β = 1, 2, 4, 8, 16.**

As before, verification of the thermal model was performed by comparing the power necessary to melt the tantalate to that predicted by the model. Good correlation was observed, however, the nearly 1000°C temperature difference between $T_c$ and $T_{mp}$ required additional model verification at the much lower $T_c$. To do this, a test sample of tantalate was patterned with 3mm long electrodes separated by 200μm. Processing proceeded by exposing pairs of spots at laser powers bracketing the expected poling power. For each laser power, two spots were exposed in which each spot differed only in the

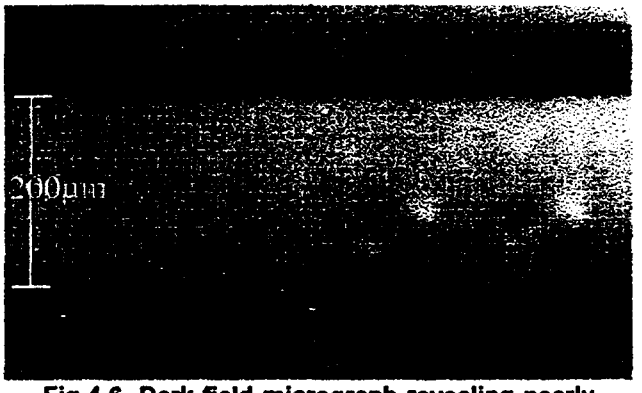


**Fig.4-6. Dark field micrograph revealing nearly circular strain associated with inverted domain boundaries. The use of this non-destructive inspection technique is an important verification of poling before proceeding with APE™ waveguide processing.**

direction of the applied 10,000 V/cm poling bias. Since, one expects a certain amount of strain associated with the boundary between the inverted domain and the original material, the sample was inspected with a dark field microscope. The nearly circular strain regions depicted in Fig. 4-6, not only provide "fine-tuned" verification of the thermal model but also since these strain patterns do not occur for lower powers, there is good evidence that these poling before proceeding with APE™ waveguide processing features are a result of the inverted domains only. In light of the fact that the typical technique for characterizing the domains is a destructive etch process, this figure illustrates *the importance of dark field inspection as a non-destructive verification technique before proceeding with waveguide processing.*

Once, the thermal model for $LiTaO_3$ had been verified, we were then able to calculate the optimum spot size/laser power combination to achieve a domain with the steepest domain walls. By appropriately choosing the poling power density such that the Curie temperature radius coincides with the point at which the second derivative of the beam intensity profile equals zero, domain wall position errors attributed to poling power variations can be minimized. Fortunately, owing to the nearly 1/z dependence of the temperature as a function of depth [10], this point roughly corresponds to the power at which the steepest domain profile is

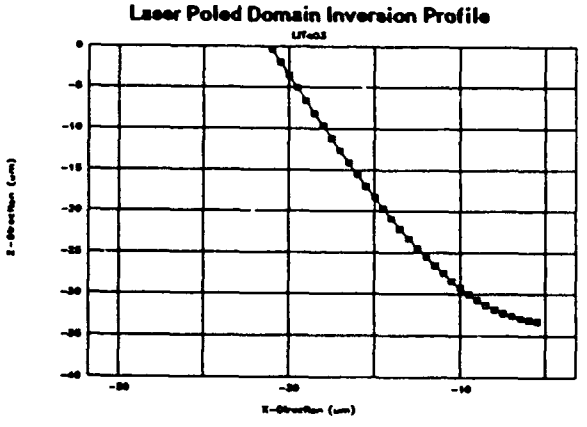


**Fig. 4-7 Calculated inverted domain profile for $LiTaO_3$. Laser poling power of 340mW in a 63μm spot produces a domain nearly 34μm deep with ~36° domain walls.**

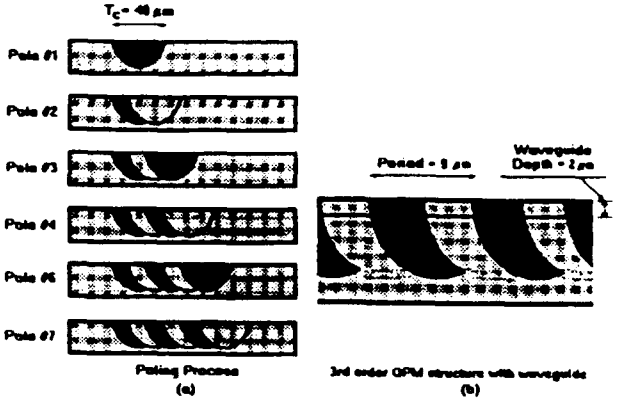

**Fig. 4-8. (a) The UTRC thermo-electric process involves iteratively "writing" an inverted domain, moving the substrate a distance corresponding to half the period and re-inverting a portion of the domain to its original orientation. (b) The resulting domain profiles appears cresent shaped.**

obtained. Optimizing the power for best possible domain profile, the poling power was calculated to be 340mW for a 63μm spot. With these parameters, the Curie temperature radius is nearly 33μm at the surface and the domain depth is ~34μm. Half of the domain inversion profile (the region above and to the right of the curve) is depicted in Fig. 4-7. As will be discussed in the next section, the 36° domain wall angle measured with respect to the vertical, represents the best achievable with the present technique.

### 4.1.4 QPM Grating Fabrication

Grating fabrication begins by patterning a 1 inch x 1 inch wafer of x-cut $LiTaO_3$ with electrodes for 100 QPM SHG devices. Each electrode pair, separated by 200 μm, extends 3 mm in the y-direction. From the previously discussed thermal model, the appropriate laser power and spot size is chosen to heat a small region of substrate surface between the electrodes. Once, thermal steady state is achieved (2s) an electric bias field of 10,000 V/cm is applied and is left on during a 2 second cooling cycle. The QPM writing process continues by moving the substrate along the y-direction corresponding to one pole width (half the grating period) and repeating the heating/cooling process with the exception of reversing the bias field in order

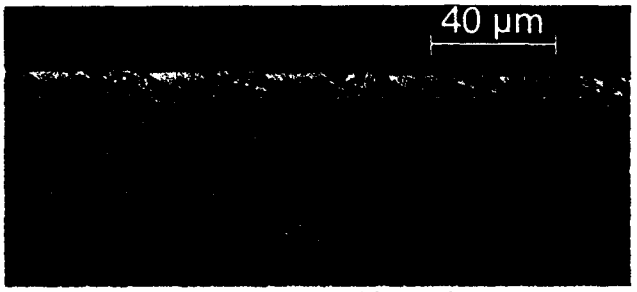


**Fig. 4-9. Preferential etching of the cross section of a QPM grating fabricated with the thermo-electric poling process reveals sharp and well defined boundaries indicating 100% complete domain inversion. The 40µm period shows extremely good uniformity and depth.**

to reverse the direction of the polarization axis. As illustrated in Fig. 4-8a, the QPM structure is produced by sequentially "freezing" out the desired domain orientation along the trailing edge of the heating beam. In this way, pole dimensions appreciably smaller than the $T_c$ diameter of the impinging beam can be produced without sacrificing domain profile. Achieving lowest order gratings with near optimum profile, ensures a strong overlap between the guided mode and the domain inverted regions which in turn allows for maximum SHG conversion efficiency. As shown in Fig. 4-8b, the resulting series of domain profiles should appear "crescent" shaped as predicted by the thermal model. However, when compared to the dimensions of the waveguide, the domain wall profile in the waveguide region can be considered nearly linear with a tilt angle of ~36°.

The photograph in Fig. 4-9, depicts a cross section of a substrate in which a 40 µm period QPM structure has been diced, polished and then processed with a preferential etch which reveals the –c face and leaves the +c face untouched. The most striking feature of the QPM grating cross section is the sharpness and definition of the individual domains. Closer inspection of the material between the etched regions reveals an extremely uniform and featureless profile indicating the thermal poling process is 100% complete. This finding is even more surprising when one considers the poling technique to produce these structures may "write" and "rewrite" any given domain four or five times as the substrate moves under the heating beam.

The tilt angle and domain depth for this device is not nearly as vertical nor as deep as predicted by the thermal model. This is presumably a consequence of this device being processed using an alternate thermal fabrication technique in which the poling beam continuously scans the grating as the bias field is switched back and forth at a steady rate. Consequently, the poor depth penetration and degraded domain profile of the "dynamic" writing approach was dropped in favor of the "steady state" technique.

### 4.1.5 QPM SHG Results

To demonstrate the applicability of the technique in the manufacture of high efficiency QPM SHG devices, 3rd order, 3mm long QPM waveguide frequency doublers were fabricated in $LiTaO_3$. In order to further define the QPM parameters, devices with QPM periods of 9, 10 and 11 µms in which waveguide widths ranging from 3 to 4µms in 0.2 µm steps were processed. Optical testing of these devices involved coupling 25mW of the output of a Ti:Sapphire laser tuned through 800-950nm. All of the QPM structures poled using this technique produced an appreciably second harmonic component. **It is important to note that for measurements of the control waveguides in which QPM gratings were not produced, second harmonic generation was not** observed. This in conjunction with the doubled component following a square law dependence on the coupled pump power and the lack of any measurable spectral broadening of the output is convincing evidence of QPM SHG. Although, the conversion efficiencies of the doublers were generally low, they are comparable to numbers typically reported in the literature for preliminary laboratory results. **The best device pumped with 25mW of 880nm light produced nearly 2µW of 440nm light corresponding to a normalized conversion efficiency of 3.6% W·cm$^{-2}$.**

### 4.1.6 QPM SHG Analysis

Since, the phase matching term in the power conversion efficiency expression goes as $\mathrm{sinc}^2(\Delta kL/2)$ where $\Delta k \equiv k_2 - 2k_1 - 2\pi m/\Lambda$, we may use the fact that this factor is reduced to ½ when $\Delta kL/2 = 0.4429\pi$ to find the full width at half maximum (FWHM) acceptance bandwidths for several

quantities as $\Delta k$ is varied.[11] Making the substitutions, the spectral acceptance bandwidth is given by:

$$\lambda = \frac{0.4429\lambda}{L}\left[\frac{n_2 - n_1}{\lambda} + \frac{\delta n_1}{\delta\lambda} - \frac{1}{2}\frac{\delta n_2}{\delta\lambda}\right]^{-1} \quad (4\text{-}1)$$

Where L is the grating length, $\lambda$ is the fundamental wavelength and $n_1$ and $n_2$ are the indices at the fundamental and second harmonic, respectively. The indices and dispersion can be calculated numerically from a Sellmeir fit for the material and the derivatives are evaluated at their respective wavelengths. For a 3mm long QPM grating in $LiTaO_3$, one expects the FWHM spectral bandwidths from eq. (1) to be on the order of 0.05nm. Instead we have observed acceptance bandwidths two orders of magnitude larger. A likely explanation for these excessive bandwidths which also can lead to the relatively low conversion efficiency observed for these devices, can be attributed to domain wall position errors. These are most likely a result of quantization errors caused by the coarse resolution of the stepper stage used for processing these preliminary devices.

As with the spectral FWHM bandwidth, the rms tolerances for the domain duty cycle and periodicity errors can be calculated. Once again, we stipulate that if the efficiency is to remain within 50% of the ideal, we require $\Phi_M = \Delta k' \, q/2 < 0.4429\pi$, where $\Delta k' \equiv k_2 - 2k_1 = \pi d_c$~ is the wave vector mismatch due to the material dispersion and $q$ *is* the increment in domain length stipulated by the translation stage. Substituting, we find:

$$q \le 0.89 l_c \quad (4\text{-}2)$$

Since, $l_c = \lambda/4(n_2 - n_1)$, $q$ must be no greater than ~2μm. For the stepper stages used in this experiment, this accounts for a reduction of some tens of a percent. This effect however, can be reduced significantly by designing the device to operate at a wavelength which requires a domain period which is an integral number of quantization increments.

In addition to the systematic errors imposed by the stepper stage, random errors of the domain position resulting from power fluctuations of the poling beam and translation stage positional accuracy can broaden the acceptance bandwidth. Assuming a statistical distribution of domain wall positions with perfect periodicity, one calculates the tolerance on the rms duty cycle error for > 50% conversion efficiency to be:

$$\sigma_l \le l_c \frac{\sqrt{2\ln 2}}{\pi} \quad (4\text{-}3)$$

For these devices, we calculate the rms duty cycle tolerance be less than 0.87μm. And in general we see that the sensitivity to duty cycle errors is rather small, with rms errors as large as one third the coherence length reducing the efficiency by less than 50 %.

For random period errors, the random walk accumulation of phase error leads to substantially greater degradation. From the analysis, the FWHM periodicity tolerance is approximately:

$$\sigma_l \le 0.72 \frac{l_c}{\sqrt{N}} \quad (4\text{-}4)$$

where $N$ is the total number of domains. **For our test devices where L = 3mm and m = 3rd order, we calculate the rms period errors to be 0.05μm!** As mentioned previously, this amounts to exacting control of both the poling laser power and stepper driven stages. For a 33μm poling spot, power amplitude fluctuations must be managed to better than 0.2%. Unfortunately, at the time these devices were processed the experimental setup incorporated stages of 0.1μm resolution and accuracy. In order to attain these tolerances we have improved control of the poling laser power by a factor of 5 and have reconfigured our poling setup to incorporate a translation stage with 30nm resolution. With these improvements, we anticipate a marked improvement in conversion efficiency.

### 4.1.7 Effect of Domain Wall Tilt on SHG Efficiency

From the onset of this program, we have stressed the importance of achieving a nearly vertical domain wall boundary in order to accomplish efficient QPM SHG. For Ti diffused $LiNbO_3$, where the tilt angle is quite large and the domain depth is dependent on the period, thermal-electric poling appears to offer clear advantages especially in the

ability to obtain period independent, deep domain inversion. Intuitively, the roughly parallelogram domain geometry and ~36° tilt angles provided by thermal poling as illustrated in Fig. 4-8b, offer an obvious improvement over the current Ti diffused $LiNbO_3$ technology. However, the nearly one for one aspect ratio between the waveguide depth and the phase matching period, makes the effect of domain tilt angle extremely deleterious. To illustrate this effect, we have simplified the typical coupled mode calculation [12] by assuming a flat-topped mode profile and have calculated the Fourier integral for a periodic grating of linear domain walls tilted at ~36°. This simple model yields:

$$d_{eff} = \frac{L}{x_o} \cdot \frac{\sin\left(\frac{3\pi x_o}{L} \cdot \tan\phi\right)}{3\pi \tan\phi} \cdot d_{ideal} \qquad (4\text{-}5)$$

where $L$ is the domain period, $x_0$ the waveguide depth, and $\phi$ the domain wall tilt angle with respect to the vertical direction. Since, the QPM SHG conversion efficiency goes as $(d_{eff})^2$, Fig. 4-10 shows a plot of $(d_{eff}/d_{ideal})^2$ versus tilt angle for a QPM grating with 3.6μm period and 4μm waveguide depth. The degree of conversion efficiency degradation is readily apparent from the figure. In fact, this simplistic model predicts for **gratings with tilt angles of 36°, the conversion**

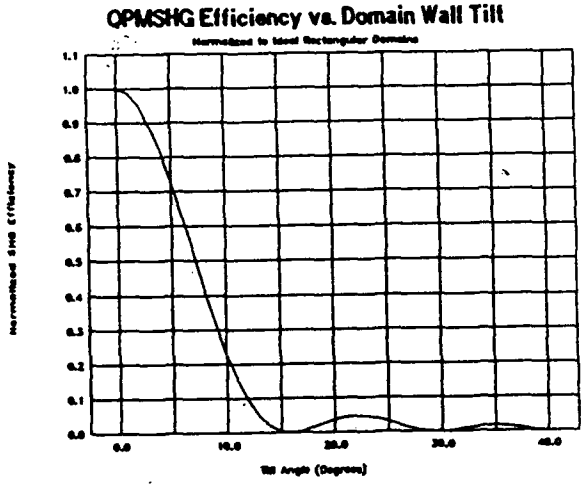


**Fig. 4-10. Reduction in QPM SHG efficiency as a function of domain wall tilt angle normalized to the efficiency of ideal rectangular domains. Grating period is 3.6μm and a flat-topped mode profile of 4μm is assumed.**

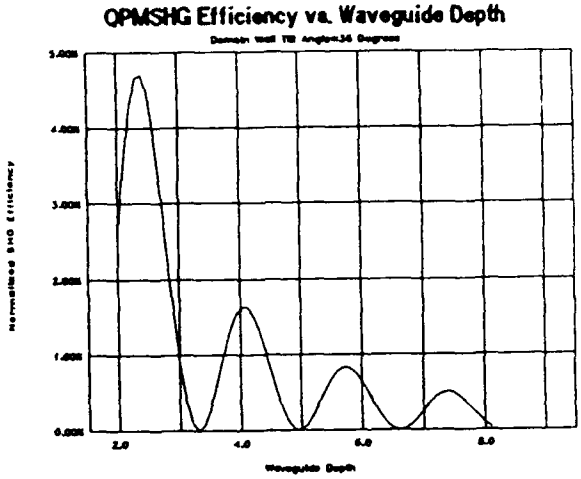


**Fig. 4-11. Optimization of flat-topped mode profile depth in order to maximize QPM SHG efficiency given the constraints of period and domain tilt of 36°.**

**efficiency has gone through two maxima and has been reduced to 1.5% of the ideal case!** Since L is fixed by the dispersion of the material and the tilt angle of 36° is the best achievable with the present technique, the only variable left to optimize the SHG efficiency is the waveguide depth. As illustrated in Fig. 4-11, a waveguide depth of ~2.4μm will increase the SHG efficiency to nearly 5% of that provided by ideal rectangular geometry domains. Recalling that efficiency goes inversely as the order number squared, *the 20 fold decrease in SHG conversion efficiency attributed to tilt angle predicted by this simplistic model, clearly illustrates the importance of fabricating first order QPM gratings.*

A consequence of assuming a flat-topped waveguide mode profile model in order to simplify the coupled mode theory, does have its limitations. This model does not accurately represent the effect of a tightly confined, nearly gaussian mode profile. Intuitively, one expects as the mode confinement increases, the period/mode-depth aspect ratio increases and the tilt angle effects on SHG conversion efficiency are related. Correspondingly, the numbers illustrated in Figs. 4-10 & 4-11, represent a worst case estimate of the tilt angle degradation of conversion efficiency.

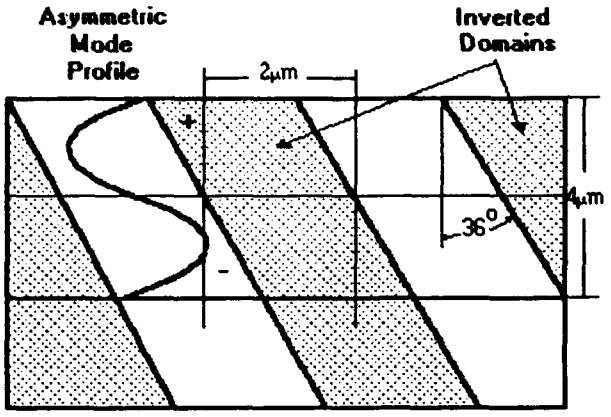


**Fig. 4-12. Domain wall tilt angle induced depth dependent phase delay, may enhance QPM SHG performance for vertically asymmetric, second harmonic mode profiles.**

Alternatively, when designing a tilt angle insensitive QPM grating, one must not ignore the increased optical losses at the fundamental wavelength, encountered when the waveguide mode profiles are much less than 3μm. A possible solution to the profile/loss compromise, depending on the system application, may be to fabricate QPM gratings with vertical waveguide dimensions large enough to support $TM_{01}$ at the second harmonic wavelength as illustrated in Fig. 4-12. Since domain wall tilt can be thought of as a possible mechanism to produce a phase delay in the upper portion of the waveguide which lags (leads) the bottom portion, one can envision an appropriate combination of domain wall tilt angle and a waveguide depth necessary to support the vertically asymmetric mode for the 2ω light, in order to take advantage of the depth dependent phase delay for enhanced overall QPM SHG efficiency. For Ti diffused $LiNbO_3$ QPM SHG, there is some evidence in the literature which supports this scheme for enhanced SHG conversion efficiency for higher order modes[13].

### 4.1.8 Thermo-Electric Poling Conclusions

The progress in *Phase I* of this program towards developing an advanced materials processing technique for integrated-optic frequency doubling, has shown promise in demonstrating efficient first order QPM SHG structures in $LiTaO_3$. Although our attempts at poling $LiNbO_3$ failed, we have successfully written 3rd order QPM gratings in $LiTaO_3$ using a novel thermal-electric poling technique. Subsequent processing of these devices with low loss APE™ waveguides has demonstrated QPM SHG results on a par with other poling methods at this stage of development.

However, the deleterious effect of the domain wall tilt associated with this technique in conjunction with this being a serial process not amenable to mass production techniques, led us to rethink further pursuing this approach in light of the highly successful e-beam poling technique currently being developed for the fabrication of QPM gratings in z-cut material. In section 4-2 which follows, we describe an e-beam technique developed at UTRC to pole x-cut $LiNbO_3$ and $LiTaO_3$.

### 4.2 Electron Beam Poling of X-Cut $LiNbO_3$

In a poled crystal of $LiNbO_3$ there is an ordered sequence of Li and Nb ions and a vacancy in the Z direction. In the +Z direction, the sequence is Nb-vacancy-Li-Nb-vacancy-Li, etc. Inverting the poling amounts to interchanging the Li ion and the vacancy, i.e., vacancy-Nb-Li-vacancy-Nb-Li, etc. At temperatures above the Curie temperature, $T_c$ = 1140°C, the poling can be reversed by application of a dc electric field with a polarity opposite the original poling field. Numerous techniques have been reported for reversing the polarization at temperatures below $T_c$ using high electric fields or combinations of electric fields and electron beam irradiation.

Second harmonic generation (SHG) devices, fabricated in Z-cut $LiNbO_3$ using domain inversion by electron-beam writing at room temperature, have been demonstrated.[15-20] A typical arrangement for domain reversal by electron beam lithography is shown in Fig. 4-13. A Z-cut substrate of $LiNbO_3$ is metalized on the +Z face and is grounded. An electron source with ~20 KeV accelerating potential and 100 to 1000 pA of current is then used to write the desired pattern of domain invertad regions directly on the -Z face. No masking is necessary so there is great flexibility in designing and executing the pattern. Also, since no heat or applied voltages are required, the method is quite straightforward.

Domain inversion at room temperature by electron-beam (without applying external electric fields) is thought to result from the combination of the high electric field produced by the electrons injected into the surface of the crystal and the excitation of the crystal lattice by the energetic beam of electrons.[21] Because $LiNbO_3$ is a very good insulator, high electric fields can be generated by the electron space charge. Such fields can be high enough, in fact, to cause mechanical damage to the crystal.

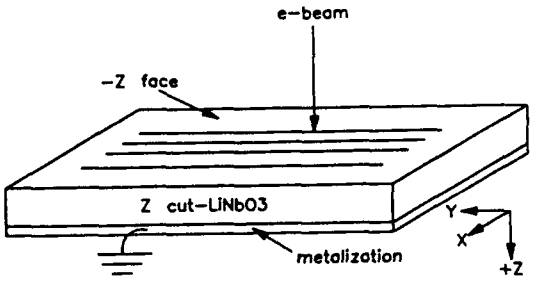


**Fig. 4-13. Domain reversal by electron-beam writing on Z-cut $LiNbO_3$**

When electrons are injected into the -Z face, the electric field generated ($E_e$) is in the direction opposite that of the polarization field ($E_p$). With a high enough electron dose, the magnitude of $E_e$ can be made equal or greater than $E_p$, and $E_e$ functions like a local poling field. At the same time, the energetic electrons excite the crystal lattice, making it easier for the Li ion to move through the triangle of oxygen ions to the vacancy site. Once this process is initiated at the surface, it propagates along the Z axis deeper into the crystal. This propagation of the domain reversal is quite dramatic as it can be accomplished with very little spreading of the domain in the lateral directions. Domain reversal gratings with a 7.5 μm periodicity have been detected on the +Z face of a 500 μm thick $LiNbO_3$ substrate after electron-beam writing on the -Z face.[17]

#### 4.2.1 E-Beam Poling of X-Cut $LiNbO_3$ or $LiTaO_3$

It is desired to create, on the surface of an X-cut crystal, a region extending along the Y axis in which the polarization is periodically reversed as shown in Fig. 4-14. A waveguide can then be created in this region to produce the SHG device. Building upon the results of the work on Z-cut $LiNbO_3$, a technique was devised at UTRC that will allow one to pole shallow regions near the surface of an X-cut crystal with an electron-beam and achieve the desired structure. The technique is to form a mesa a few microns high by ion beam etching the X surface such that the sides of the mesa, if vertical, would be +Z and -Z surfaces. Figure 4-15 shows a schematic of this configuration. If the +Z side is metalized and grounded, and an electron-beam is directed onto the -Z side of the mesa, the geometry

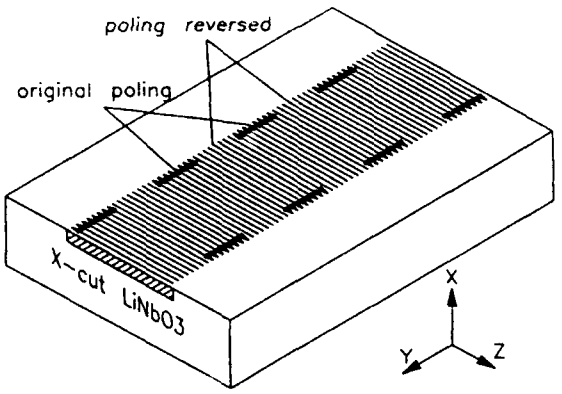


**Fig. 4-14 Periodic poling on X-cut $LiNbO_3$ for QPM SHG devices**

used in the experiments on Z-cut material is approximated. With the correct dosage and accelerating potential, the direction of the poling can be reversed.

The goal of this part of the program was to demonstrate that the above is a viable method for achieving electron-beam poling on X-cut $LiNbO_3$ and $LiTaO_3$ for SHG applications. Demonstration of polarization reversal is the first step, with the fabrication of periodically poled SHG structures and demonstration of SHG to follow.

### 4.2.2 Experimental Technique

Though the optical damage threshold for $LiTaO_3$ is superior to waveguides fabricated in niobate (making it the material of choice for frequency doubling), $LiNbO_3$ was used throughout these experiments owing to its availibility and lower cost. It is assumed that once the technique is demonstrated in niobate, the similarity in stochiometric composition between the two materials will allow for a relatively straightforward extrapolation of the technique to tantalate. With this in mind, it is the authors' intent that reference to niobate in the discussion that follows, applies equally well to tantalate with some qualifications.

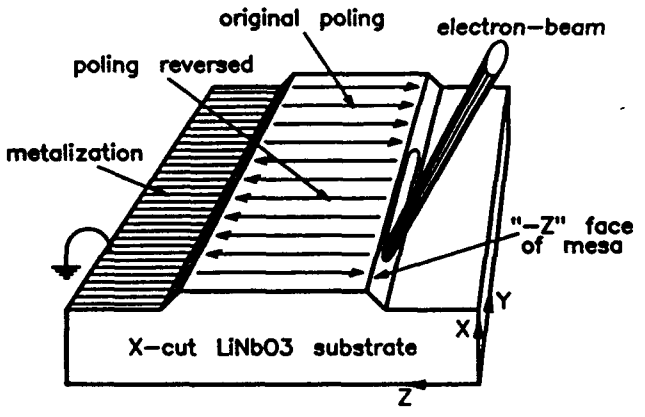


**Fig. 4-15. UTRC configuration for electron-beam poling of X-cut $LiNbO_3$**

#### 4.2.2a Mesa Formation

$LiNbO_3$ substrates were X-oriented, 1 inch long in the Y and Z directions, and 0.51 mm in thickness. Because $LiNbO_3$ is not readily chemically etched, the mesas were formed by argon ion beam milling. Mesas 2.5 to 3.0 μm in height were milled in approximately 1 hour. In order to increase the slope of the -Z side of the mesa to more closely approximate a -Z surface, substrates were oriented (X-axis or surface normal) at 80° to the beam of ions during milling and were not rotated during the ion beam exposure. This produced a slope of ≈70° on the -Z side of the mesa and a slope of ≈30° on the +Z side as shown in Fig. 4-16. The steeper slope on the -Z face leads to $E_e$ having a larger component directly opposing $E_p$. It is this cosine component of $E_e$ that plays a major role in inverting the polarization. The mesa slopes are important for a second reason. That is, it is necessary to metalize the +Z slope in order to provide a ground reference for $E_e$, and the more shallow slope makes it easier to obtain a continuous metalization up the side of the mesa.

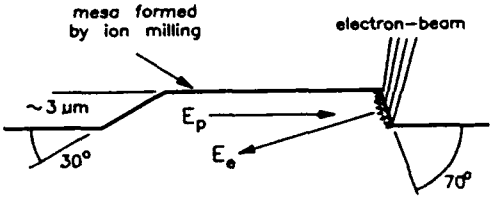


**Fig. 4-16. $LiNbO_3$ mesa geometry and electric fields during e-beam domain inversion.**

The process of learning the best technique for ion beam etching relatively deep mesas in $LiNbO_3$ consumed a number of substrates. Lithium niobate is

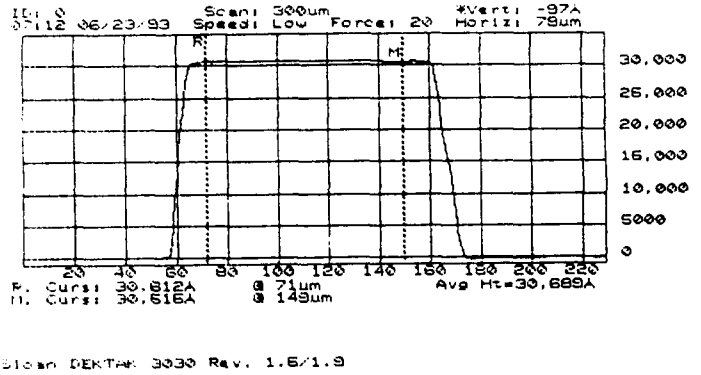


**Fig. 4-17. Dektak scan of 100μm wide, 3μm high ion milled mesa.**

not only very resistant to chemical etching, but as an oxide, has a rather slow ion beam etch rate (~30 nm/min). It was therefore necessary to find a masking material: (1) that had a significantly slower etch rate than $LiNbO_3$ so that the mask material could protect the mesas while the surrounding $LiNbO_3$ was being etched away, and (2) whose sidewall slope could be controlled so that the desired mesa edge definition and mesa slopes could be obtained.

The procedure that was devised employed a masking film of aluminum, and the ion milling was carried out with a partial pressure of oxygen to convert the Al to Al oxide during the milling process. The etch rate of Al oxide is ~7 nm/min, and an Al film thickness of ~2μm was used to insure that there would be some mask material left when the $LiNbO_3$ mesa height reached 3μm. The Al mesa mask pattern was defined in the Al film by applying a 1μm photoresist layer, UV-exposing the photoresist using the IOFD-3 mesa photomask, and then etching the Al with a combination of chemical etching followed by ion milling so as to control the sidewall profile. Chemical etching alone would have led to excessive undercutting of the Al and to very shallow $LiNbO_3$ mesa slopes. Figure 4-17 is a Dektak scan over one of the 100μm wide mesas showing the 3 μm height of the mesa and the difference in the +Z and -Z slopes.

### 4.2.2b Metalization

Once the mesas were ion milled, the substrate was then metalized using the IOFD-3 metalization mask. The purpose of the metalization was to provide a ground reference for the electron-beam injected space charge, and to provide a return path for excess charge to ground. Photolithography on transparent substrates, such as $LiNbO_3$, and particularly transparent substrates with significant surface topology, i.e. 3μm high mesas, requires that special techniques be used to minimize reflections during the photoresist exposure process. In order to obtain good pattern definition in this situation: (1) non-reflecting fixturing must be employed in the UV-exposure apparatus, and (2) a photoresist that incorporates an absorbing dye must be used. With these two precautions, the metalization of the substrates for the poling experiment was straightforward. Both aluminum and gold were used for the metal, with typical thicknesses being ~ 200nm.

Figures 4-18 and 4-19 show features of the metalization pattern that was deposited onto the $LiNbO_3$ substrates after ion milling. The photomask set used in this work was designated as IOFD-3 and the entire pattern contained 18 mesas, labeled A thru R. Mesas A thru F were 50μm wide, mesas G thru L were 100μm wide, and mesas M thru R were 20μm in width. Each mesa was 20mm long and contained 20 "experiments". Each experiment was 500μm long with two versions: (1) with 6μm fingers and spaces, and (2) a continuous ground metalization. The finger pattern was designed to determine the influence of a

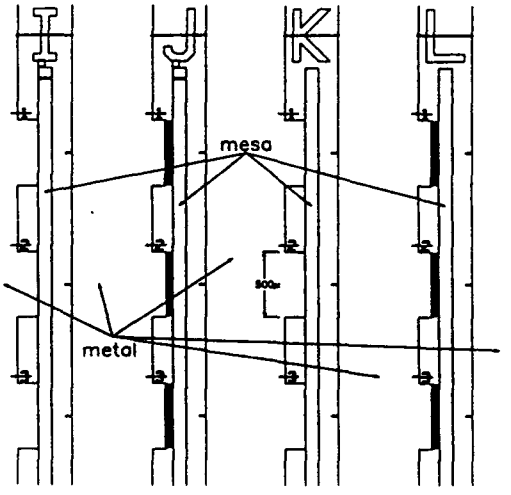


**Fig. 4-18. Portion of IOFD-3 mask set showing mesas and metalization pattern.**

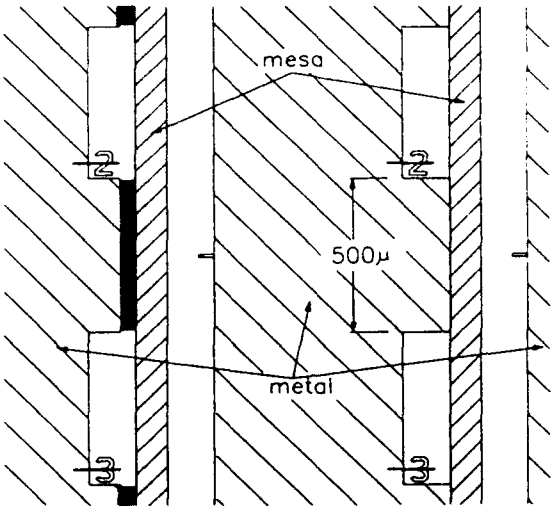


**Fig.4-19. Detail of IOFD-3 mask set showing solid and interdigitated ground metal patterns.**

ground on the geometry of the poled region. That is, could the periodicity of the poling be controlled by a ground metal pattern or was it necessary to modulate the electron-beam on and off to produce a periodic poling reversal?

### 4.2.2c Electron-beam writing

The relatively large number of experiments on each mesa was necessary because the dosage required to obtain domain reversal was not accurately known apriori. Dosages calculated from the literature [16, 18, 19, 20] vary from less than 100μC/cm$^2$ to almost 20,000μC/cm$^2$. Hsu[18] gives some of the most complete data, including the dependence of the depth of the inverted domain upon electron-beam current and scan rate. From [18], for a current of 600pA and for a 100μm wide mesa, a dose of 1,700μC/cm$^2$ was calculated. Using this as a guide, the dosage applied in the experiments of this work varied from ~100μC/cm$^2$ to over 6,000μ C/cm$^2$. Mechanical damage to the substrate, an example of which is shown in Fig. 4-20, was found to occur for electron doses above ~8,000μC/cm$^2$. Domain reversal by electron-beam must take place below the damage threshold for this to be a useful technique.

An electron-beam potential of 20 KeV was used in these experiments. This electron energy is typical of the referenced work and, from a plot of electron penetration range in terms of material density versus electron energy [22], should provide for an electron injection depth of ~1μm into $LiNbO_3$.

Direct electron-beam writing was achieved using a scanning electron microscope (SEM). It was originally intended that the ISI SR50 SEM in the UTRC microelectronics laboratory would be used for this work. This SEM is fitted with a beam blanker and a *Tracor Northern* electron-beam lithography system and is capable of the accelerating potentials and beam currents required for this experiment. However, the ISI SEM was not originally designed for electron-beam writing and, while modified to be suitable for some writing tasks where registration with an existing pattern is not required, was found to be unsuitable for the present poling experiments.

This conclusion was reached only after a substantial amount of effort was expended in developing fixturing for the ISI SEM, preparing substrates for calibration and setup, and learning the capabilities and limitations of the machine. A satisfactory method of alligning the position of the 20 KeV electron-beam with respect to features of the substrate without exposing the substrate to high doses of 20 KeV electrons was not established. The

**Fig. 4-20. Photo of device E1 showing mechanical damage due to excess electron dosage.**

difficulty is trying to insure that electrons are being injected into the desired -Z slope of the mesa during the writing operation without some previous, undesired exposure having occurred during the alignment proceedure. Attempts were made to do the allignment to the substrate at low electron energies (1 KeV) where charge build-up was minimal, and then switch to 20 KeV for the writing. However, the mechanical configuration of the ISI SEM is such that the focal point of the electron-beam is not, in general, independent of electron energy. In fact, the focal points at 1 and 20 KeV were usually so far apart that they did not appear on the screen at the same time at magnifications required to establish the desired allignment. The conclusion arrived at was that another SEM, one specifically designed or modified for electron-beam writing, was needed for this job.

Through the cooperation of Professor Mark Reed and graduate student Jeff Sleight of the Yale University Department of Electrical Engineering, the final 2 $LiNbO_3$ samples processed during this program were electron-beam exposed in the *Joel* JSM-6400 SEM at Yale's Becton Center. This SEM was specifically adapted for electron-beam writing, and is capable of writing 30 nm features, and has more than adequate accelerating potential range and current capability for the poling experiment. The Yale SEM is also fitted with an optical microscope that can be used for allignment. This is an extremely important feature in the poling experiment since it allows for precise allignment to the -Z mesa edge without exposing the $LiNbO_3$ sample to the electron-beam.

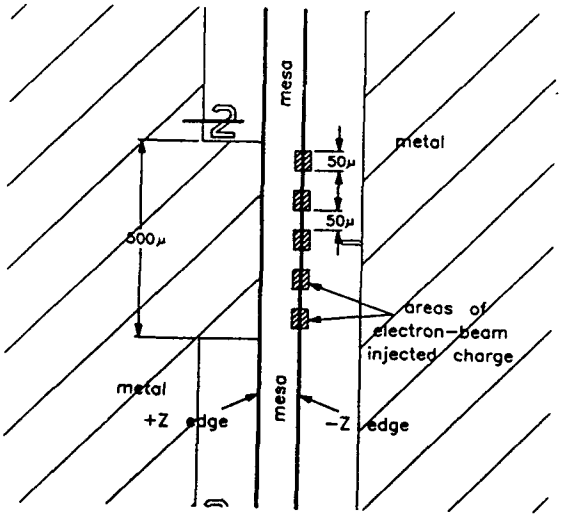


**Fig. 4-21. Electron-beam exposure pattern on $LiNbO_3$ substrate.**

The electron-beam pattern written at each experiment site on the first of the two $LiNbO_3$ substrates (designated as Y1) exposed at Yale consisted of a sequence of 40μm wide (Z direction) by 50μm long (Y direction) exposures separated by 50μm spaces as shown in Figure 4-21. The width of the exposure area in the Z direction was larger than desired but was used because of a temporary alignment difficulty and a less than complete understanding between UTRC and Yale of the preferred exposure geometry. Both situations were corrected, and the electron-beam pattern exposure of the second substrate (designated as Y2) was nearly ideal with less than 2um overlap onto either the top of the mesa or the level below the mesa. The same exposure pattern was used in the Y direction, i.e. 50 μm long exposed areas separated by 50μm unexposed areas. An electron energy of 20KeV was used for both of these substrates and the dosage varied on each column of 20 experiments from a low of 88μC/cm$^2$ to a high of 6,086μC/cm$^2$

### 4.2.3 Discussion of E-Beam Poling Results

As a standard practice, domain reversal in Z-cut material, is revealed by etching the +Z face of the crystal with a HF-$HNO_3$ mixture which preferentially attacks the -Z face. Therefore, regions where the poling was reversed, exposing a +Z surface to the etchant reveals the -Z domains. In the present case, because the regions where one is attempting to reverse the poling are but a few microns in depth, verification of a successful experiment is more difficult. The areas in which the poling is reversed lie within the height of the mesas, or within about 3 μm from the surface. Therefore, in order to be able to detect poling reversal using the preferential etching technique (see Fig. 4-22), it is

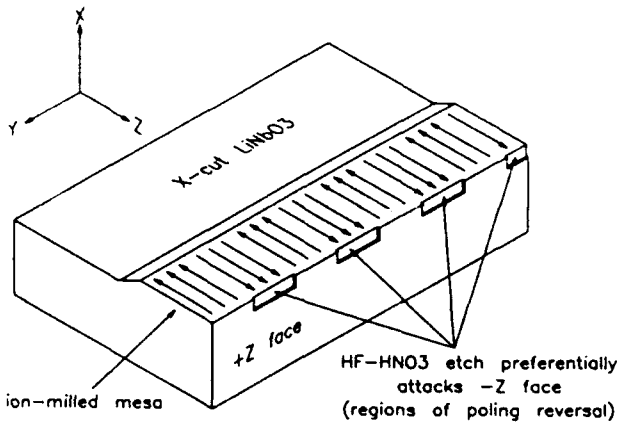


**Fig. 4-22. Illustration of preferential etching to reveal domain reversal.**

necessary to first cut and polish the substrate in such a way as to expose the +Z face of the crystal and also preserve the poled areas adjacent to the X surface.

Substrates Y1 and Y2 were cut and polished along the length of one of the 100μm wide mesas: the K mesa on substrate Y1 and the L mesa on substrate Y2. The polished pieces were then etched in 2 parts $HNO_3$ and 1 part HF at 90°C for 30 minutes and examined under a microscope for indications of preferential etching and polarization reversal.

Figures 4-23 and 4-24 show the effects of the $HNO_3$-HF etch, on experiment site L3 on substrate Y2. Site L3 received an electron dose of 3,900μ $C/cm^2$. The areas that have been eroded by the etch correspond to the 3 μm depth of the mesa and the 50 μm on-and-off geometry of the electron deposition pattern. The columnar structure revealed in the top view of the substrate (Fig. 4-24) indicates that the polarization reversal occurred across the entire width of the mesa.

Etching of experiment site L2, which received a higher electron dose of 4,900μ$C/cm^2$, did not clearly reveal the charge deposition geometry, but was more uniformly etched, indicating that polarization reversal occurred, but that the electron dose was large enough to cause the polarization reversal to spread into the 50μm areas between the areas of charge deposition. The site receiving the highest dose, site L1, was even more uniformly etched, making recognition of the electron deposition pattern difficult. Site L4 on the lower dose side of L3 received 3,100μ$C/cm^2$ and showed no -Z face etching and hence no sign of polarization reversal. The threshold for domain reversal by electron-beam injection was therefore ~ 3,500 μ$C/cm^2$.

### 4.2.4 E-Beam Poling Conclusions

The potential for fabricating SHG devices in X-cut $LiNbO_3$ by electron-beam writing has been demonstrated. By creating mesas a few microns high on X-cut material and writing with an electron beam on the -Z like slope of the mesa, the poling has been reversed in a controlled manner. Additional work will be required in order to develop a complete understanding of electron-beam poling process and to gain knowledge of the optimum parameters for producing periodically poled devices foe SHG applications.

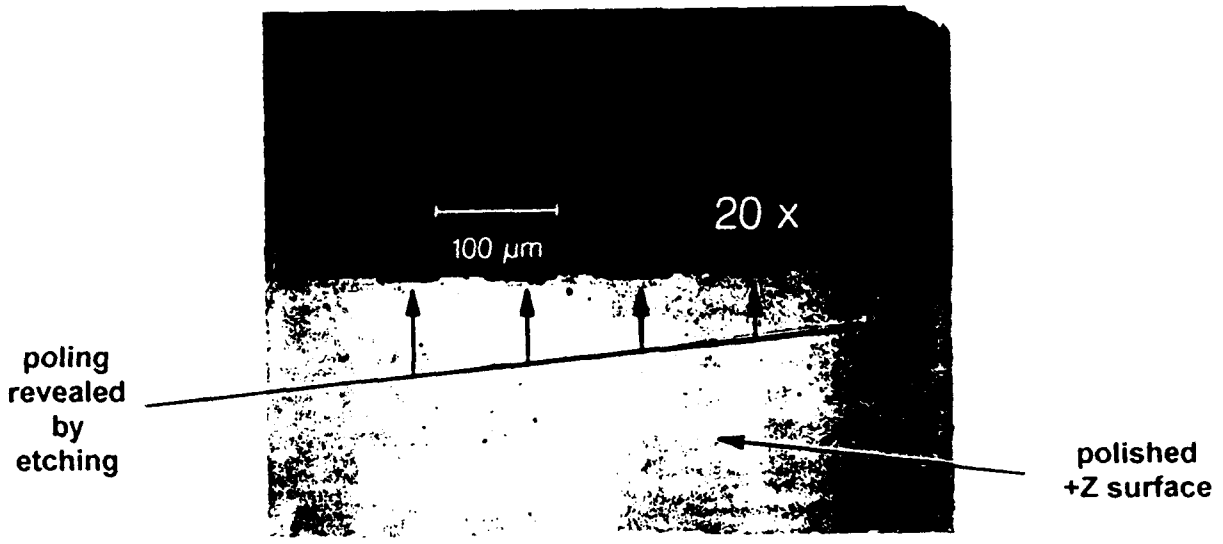


**Fig. 4-23. Cross-sectional view of site L3 on substrate Y2 showing effects of preferential etching.**

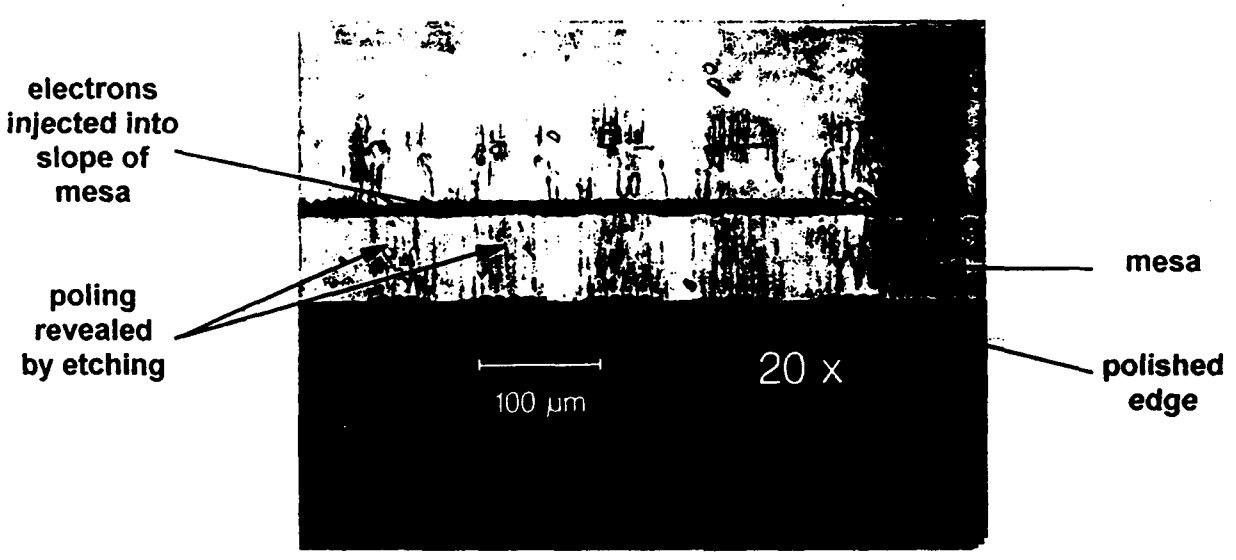


**Fig. 4-24. Top view of site L3 on substrate Y2 showing effects of preferential etching.**

## 5.0 SUMMARY

This effort represents the only on-going work in processing of QPM frequency doublers in x-cut material. There remains a compelling motivation for developing frequency doublers in this crystallagraphic orientation in that it is generally recognized in the photonics community, that x-cut $LiNbO_3$ and $LiTaO_3$ yields integrated-optic devices with superior operational and environmental characteristics over their z-cut counterparts. From an integrated-optic (IO) point of view, this material not only allows for on-chip integration of high performance IO devices such as phase and intensity modulators, but is also the correct orientation for direct coupling of high power, heterostructure laser diode arrays.

The laser thermal-electric poling technique developed at UTRC for processing x-cut material achieved promising preliminary results. Laser poling provided a solution to the period/domain depth limitation of competing diffusion methods. However, by virtue of the this being a diffusion of heat process, we were not able to find a practical approach to correct the excessive domain wall tilt of ~36°. Moreover, the exacting tolerances imposed by QPM on the domain periodicity, proved difficult to achieve with serial processing of the domains, eg. SHG waveguides processed in these devices displayed excessive acceptance bandwidths (~10nm) and consequently had very low conversion efficiencies. Devices processed with improved control on stepper stage accuracy and laser amplitude stability, showed little improvement. Perhaps the most unsettling evidence that this process does not lend itself to the manufacture of efficient QPM SHG devices, is the degree of light (fundamental and second harmonic) scattering out of the plane of the QPM grating. Though, no strain induced scattering centers were observed in devices processed with this technique, it is presumed this is due to the domain wall tilt. Finally, it became clear that this technique is not amenable to high volume production techniques, compelling us to investigate e-beam polling in *Phase - II.*

The UTRC e-beam poling technique builds on the highly successful technique developed for e-beam processing of z-cut material. By ion-milling 200 μm wide by 3μm high mesas in the y-direction, electrons injected into the -z face of the mesa "see" the electrode pattern on the +z face as if the x-cut material was z-cut. We have demonstrated gross domain reversal gratings with periods of 50μm and depths of 3μm. Clearly, additional work will be required to develop a complete understanding of this process in order to optimize the parameters for producing optimum periodically poled devices for QPM SHG applications. This demonstration of e-beam poling in x-cut material is an important first step.

## REFERENCES


1. Mizuuchi, K. and K. Yamamoto: *Highly Efficient QPM SHG Using a First-Orde. Periodically Domain-Inverted $LiTaO_3$ Waveguide,* Appl. Phys. Lett., 60 (11), 16 March 1992.
2. HSN, W. and M. C. Gupta: *Domain Inversion in $LiTaO_3$ by Electron Beam,* Appl. Phys. Lett., 60 (1), 6 January 1992.
3. Yamada, M. and K. Kishima: *Fabrication of Periodically Reversed Domain Structure for SHG in $LiNbO_3$ by Direct Electron Beam Lithography at Room Temperature,* Electr. Lett., 27, (10), 9 May 1991.
4. Lim, E. J., M. M. Fejer, R. L. Byer and W. J. Kozlovsky: *Blue Light Generated by Frequency Doubling in Periodically Poled Lithium Niobate Channel Waveguides,* Electron. Lett., Vol. 25, pp. 731-732, 1989.
5. Fejer, M. M. and E. J. Lim: *Quasi-Phase-Matched Second Hannonic Generation in $LiNbO_3$ Waveguides,* **Technical Digest on Integrated Photonics Research,** 1990 (Optical Society of America, Washington, DC, 1990), Vol. 5, pp. 109-110.
6. Lim, E. J., M. M. Fejer, and R. L. Byer: *Second-Harmnonic-Generation of Green Light in Periodically Poled Planar Lithium Niobate Waveguide,* Electron. Lett., Vol. 25, pp. 174-175.
7. Lax, M.: *Temperature Rise Induced by a Laser Beam,* **Journal of Applied Physics,** Vol. 48, No. 9, pp.3919-3924, 1977.
8. Cline, H. E. and T. R. Anthony: *Heat Treating and Melting Material with a Scanning Laser or Electron Beam,* **Journal of Applied Physics,** Vol. 48, No. 9, pp.3895-3900, 1977.
9. Nissim, Y. I., A. Lietoila, R. B. Gold, and J. F. Gibbons: *Temperature Distributions produced in Semiconductors by a Scanning Elliptical or Circular CW Laser Beam.* **Journal of Applied Physics,** 51(1), pp.274-279, 1980.
10. Moody, J.E. and R. H. Hendel: *Temperature Profiles Induced by a Scanning CW Laser Beam,* **Joumal of Applied Physics,** 53(6), pp. 4364-4371, 1982.
11. Servoin, J. L. and F. Gervais: *Analysis of Infrared Reflectivity in the Presence of Asymmetrical Phonon Lines,* **Applied Optics,** Vol. 16, No. 11, pp. 2952-2956, 1977.
12. Ardvidsson, G. and B. Jaskorzynska: ...: *Influence of the Shape of the Dornain Boundary on 'QPM' Conversion Efficiency;* **Conf. Materials for Non-Linear and Electrooptics,** Cambridge, 1989.
13. Cao, X., R. Srivastava and R. V. Ramaswamy: *Efficient Quasi-Phase-Matched Blue Second-Harmonic Generation in $LiNb0_3$ Channel Waveguides by a Second-Order Grating;* **Applied Physics Letters,** Vol. 17, No. 8., 1992.
14. *Quasi-Phase-Matched Second-Harmonic Generation: Tuning Tolerances;* M. M. Fejer, G. A. Magel, D. H. Jundt and R. L. Byer, Unpublished.
15. Keys R. W., et. al., "*Fabrication of Domain Reversed Gratings for SHG in $LiNbO_3$ by Electron Beam Bombardment*", **Electronics Letters 26,** no.3, p.188, 1 Feb 1990.
16. Yamada M. and K. Kishima, "*Fabrication of Periodically Reversed Domain Structure for SHG in $LiNbO_3$ by Direct Electron Beam Lithography at Room Temperature*", **Electronics Letters 27,** no.10, p.828, 9 May 1991.
17. Ito, H., C. Takyu, and H. Inaba, "*Fabrication of Periodic Domain Grating in $LiNbO_3$ by Electron Beam Writing for Application of Nonlinear Optical Processes*", **Electronics Letters 27,** no.14, p.1221, 4 July 1991.

18. Hsu, W. and M. Gupta, "*Domain Inversion in $LiTaO_3$ by Electron Beam*", **Appl. Phys. Lett. 60** (1), p.1, 6 January 1992.

19. Nutt, A., V. Gopalan, and M. Gupta, "*Domain inversion in $LiNbO_3$ using direct electron-beam writing*", **Appl. Phys. Lett. 60** (23), p.2828, 8 June 1992.

20. Fujimura, M, T. Suhara, and H. Nishihara, "*$LiNbO_3$ Waveguide SHG Device with Ferroelectric-Domain-Inverted Grating Formed by Electron-Beam Scanning*", **Electronics Letters 28**, no.8, p.721, 9 April 1992.

21. Haycock, P. and P.Townsend, "*A method of Poling $LiNbO_3$ and $LiTaO_3$ Below $T_C$*", **Appl. Phys. Lett. 48** (11), p.698, 17 March 1986.

22. Birks, L.S., "*Electron Probe Microanalysis*", Chemical Analysis monographs ed by P.J. Elving & I.M. Kolthoff, J. Wiley & Sons, Inc., New York, p.107,1971.

23. Bhargava, R. N., "*Materials Growth and Its Impact on Devices from Wideband Gap II-VI Compunds*". **J. Crystal Growth**, Vol. 86, pp. 873-879, 1988.

24. DePuydt, J. M., M. A. Hasse, H. Cheng and J. E. Potts, "*Electrical Characterization of p-Type ZnSe*", **Appl. Phys. Lett.**, Vol. 55, pp. 110; 3-1105, 1989.

25. Somekh, S. and A. Yariv, "*Phase Matching by Periodic Modulation of the Nonlinear Optical Properties*", **Opt. Commun.**, Vol. 6, pp. 301-304, 1972.

26. Webjorn, J. F. Laurell, and G. Arvidsson, "*Blue Light Generated by Frequency Doubling of Laser Diode Light in a Lithium Niobate Channel Waveguide*", **IEEE Photonics Technology Lett.**, Vol. 1, pp. 316-318, 1989.

27. Webjorn, J. F. Laurell, and G. Arvidsson, "*Fabrication of Periodically Domain-Inverted Channel Waveguides in Lithium Niobate for Second Harmonic Generation*", **J. Lightwave Tech.**, Vol. 7, pp. 1597-1600

28. Mizuchi, K., K. Yamamoto and T. Tadiuchi, "*Second Harmonic Generation of Blue Light is a $LiTaO_3$ Waveguide*", **Appl. Phys. Lett.** 58, pp. 2732-2734, 1991.